micromachines

Article

Modeling of MEMS Transducers with Perforated Moving Electrodes

Karina Šimonová and Petr Honzík *

Faculty of Transportation Sciences, Czech Technical University in Prague, Konviktská 20, 110 00 Praha, Czech Republic; abramkar@fd.cvut.cz
* Correspondence: honzikp@fd.cvut.cz

Abstract: Microfabricated electroacoustic transducers with perforated moving plates used as microphones or acoustic sources have appeared in the literature in recent years. However, optimization of the parameters of such transducers for use in the audio frequency range requires high-precision theoretical modeling. The main objective of the paper is to provide such an analytical model of a miniature transducer with a moving electrode in the form of a perforated plate (rigid elastically supported or elastic clamped at all boundaries) loaded by an air gap surrounded by a small cavity. The formulation for the acoustic pressure field inside the air gap enables expression of the coupling of this field to the displacement field of the moving plate and to the incident acoustic pressure through the holes in the plate. The damping effects of the thermal and viscous boundary layers originating inside the air gap, the cavity, and the holes in the moving plate are also taken into account. The analytical results, namely, the acoustic pressure sensitivity of the transducer used as a microphone, are presented and compared to the numerical (FEM) results.

Keywords: analytical modeling; electroacoustic transducers; MEMS microphones; perforated plate

check for updates

Citation: Šimonová, K.; Honzík, P. Modeling of MEMS Transducers with Perforated Moving Electrodes. *Micromachines* **2023**, *14*, 921. https://doi.org/10.3390/mi14050921

Academic Editor: Libor Rufer

Received: 24 March 2023
Revised: 18 April 2023
Accepted: 20 April 2023
Published: 24 April 2023

Copyright: © 2020 by the authors. Licensee MDPI, Basel, Switzerland. This article is an open access article distributed under the terms and conditions of the Creative Commons Attribution (CC BY) license (https://creativecommons.org/licenses/by/4.0/).

1. Introduction

Currently, the vast majority of MEMS microphones production, increasing rapidly in recent years, uses the electrostatic principle of electroacoustic transduction [1] (although piezoelectric types exist [2]). Such devices consist of moving electrodes of circular [3], square [4,5], or other [6] shapes and perforated single [3] or double backplates [7,8]. Note that such MEMS structures can be employed in other domains than audio, such as energy transfer, energy harvesters, and resonators [9–11]. However, new designs presenting technological advances have been proposed recently in the literature, such as a microphone with moving microbeam [12], or transducers (sources and microphones) with perforated moving electrodes. The mean motivation for the work presented herein is the latter case with electrodes in the form of elastic perforated plates clamped at all boundaries [13] or rigid elastically supported perforated plates [14–17]. Although these experimental studies contain approximate theoretical models, mainly based on the lumped elements approach, the precise analytical modeling is still of high interest.

In order to provide high-precision results on sensitivity and bandwidth, the models of electroacoustic transducers (miniaturized or not) should take into account the damping effects of the viscous and thermal boundary layers originating in the narrow regions such as the air gap between the moving and fixed electrodes. The strong coupling between the displacement field of the moving electrode and the acoustic field inside the transducer should be also accounted for when appropriate. In addition to these effects, the model of the transducer with a perforated moving electrode has to deal with the acoustic short circuit between the incident acoustic pressure and the pressure field inside the transducer caused by the perforation. This leads to the sensitivity roll-off at lower frequencies, which has to be calculated correctly when precise theoretical modeling allowing the optimization of the transducer behavior in the audio frequency range is required.

While the precise models of the transducers with perforated moving electrodes are still missing, to our knowledge, several models taking into account the perforation of the fixed electrodes and the acoustic short circuit can be found in the literature. The classical lumped-element models of condenser microphones, such as [18], use the "porosity" approach; the more recent lumped-element model [19] deals with acoustic short circuit through the venting hole. With regard to more advanced models, ref. [20] and, more recently, [21,22] took into account the effects of holes in the fixed electrode accounting for the position of the holes, and ref. [23] employed the impedance approach. Vibration of a very thin perforated backplate of an MEMS transducer was taken into account in [24]. In [25], the effect of the acoustic short circuit through thin slits surrounding the moving electrode in the form of a microbeam was included in the complex wavenumber for the acoustic pressure in the air gap. In the same reference, the acoustic pressure in the air gap was expressed using integral formulation with appropriate Green's function, which was not expressed as a series expansion over the eigenfunctions of the moving electrode. Such a fomulation is also advantageous in the case of rectangular geometries [26,27] and is therefore used herein. It is worth mentioning the numerical methods, namely, the finite element method, which can take into account the thermoviscous losses and the coupling effects without geometry-dependent approximations [28]. However, numerical methods generally suffer from high computational costs, compared to analytical methods, and are usually used as a reference against which the analytical results can be tested.

The present paper deals mainly with the theoretical modeling of the acoustic field inside a miniaturized electroacoustic transducer with a square perforated moving electrode, taking into account its coupling with the vibration of the moving electrode, the acoustic short circuit through the perforation, and the thermoviscous losses originating in the narrow regions inside the transducer. Two types of the perforated moving electrode are considered: (i) the rigid elastically supported square plate, partially inspired by [14] (see Figure 1a), and (ii) the flexible square plate clamped at all boundaries, partially inspired by [13] (see Figure 1b).

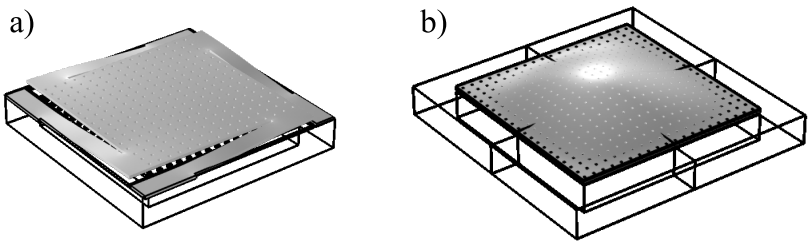

Figure 1. MEMS transducers with perforated moving electrodes in the form of (**a**) the rigid elastically supported square plate and (**b**) the flexible square plate clamped at all boundaries.

Section 2 presents viscous effects in short narrow holes and governing equations for the acoustic pressure field in the thin air gap between the perforated moving electrode and the fixed one (backplate) using the porosity approach. Then, the solutions for the acoustic pressure are expressed for the case of uniform (piston-like) and nonuniform movement of the moving electrode, corresponding to the rigid elastically supported and flexible plate, respectively. The coupling of the acoustic field with vibration of the plates of both types, leading to the expression of their displacements, is finally derived, with the eigenfunctions of the perforated flexible clamped plate being given approximately in Appendix A. In Section 3, the analytically calculated acoustic pressure sensitivities of the transducers used as microphones are depicted and compared with the numerical (FEM) results. The influence of some geometrical parameters is discussed. This section is followed by the conclusion in Section 4.

2. Analytical Solution

In this section, the analytical solution of the problem is expressed in frequency domain (the time dependence being $e^{j\omega t}$; ω is the angular frequency). The acoustic field inside the transducer and the displacement of the moving electrode is searched for as a response to harmonic incident acoustic pressure p_{inc} (assumed to be uniform over the moving electrode surface).

2.1. Description of the Device

The device consists of a moving electrode in the form of a square perforated plate of side $2a$ and thickness h_p with N square holes of side a_h, with the air gap between the plate and the backplate of thickness h_g surrounded by a peripheral cavity described by its volume V_c and acoustic impedance Z_c (see Figure 2). The perforation ratio $\mathcal{R} = Na_h^2/(4a^2)$ is the ratio of total surface occupied by the holes and the area of the plate. In the case of a moving electrode in the form of a rigid elastically supported square plate (Figure 1a), the plate displacement is uniform and the cavity is connected with the incident acoustic pressure p_{inc} through slits of thickness h_s along the arms supporting the plate.

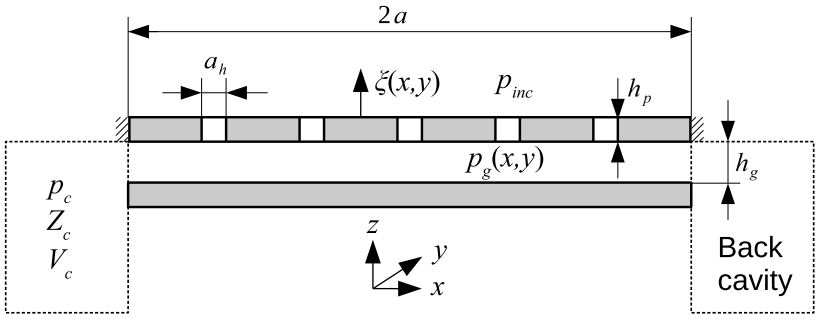

Figure 2. Sketch of the whole system.

2.2. The Acoustic Pressure Field inside the Transducer

The system is supposed to be filled with thermoviscous fluid (air in this case) with the following properties: the density ρ_0, the adiabatic speed of sound c_0, the heat capacity at constant pressure per unit mass C_p, the specific heat ratio γ, the shear viscosity coefficient μ, and the thermal conduction coefficient λ_h. Since the air gap thickness h_g is supposed to be much smaller than other dimensions of the air gap and smaller than the wavelengths considered, even at high frequencies, the acoustic pressure in the air gap is assumed to depend on the x, y spatial coordinates only and denoted $p_g(x, y)$. The particle velocity and temperature variation (that generally depend on the z axis due to the viscous and thermal boundary layers effects) are then replaced by their mean values over the air gap thickness. The acoustic pressure in the cavity volume p_c is supposed to be uniform. The displacement of the moving electrode is denoted ξ.

2.2.1. Viscous Effects Originating in the Holes in the Perforated Moving Electrode

For the sake of simplicity, the holes in the moving electrode are supposed to have circular cross-section instead of the square one, with the radius of the equivalent cylindrical hole being given by $R_h = a_h/\sqrt{\pi}$ (thus $\mathcal{R} = \frac{N\pi R_h^2}{4a^2}$), see Figure 3. The particle velocity $v_z(r, z)$ in such a hole is governed by the diffusion equation [29]

$$\left(\frac{1}{r}\frac{\partial}{\partial r}r\frac{\partial}{\partial r} + k_v^2\right)v_z(r,z) = \frac{1}{\mu}\frac{\partial}{\partial z}p(z), \tag{1}$$

with the diffusion wavenumber

$$k_v = \frac{1-j}{\sqrt{2}}\sqrt{\frac{\omega\rho_0}{\mu}}, \tag{2}$$

with j being the imaginary unit, and subjected to the nonslip boundary condition at $r = R_h$

$$v_z(R_h, z) = j\omega\xi(x, y). \tag{3}$$

The velocity of the moving electrode $j\omega\xi(x, y)$ at the position of the hole is assumed to be approximately uniform on the whole internal surface of the hole. The solution of the problem (1) and (3) is given by

$$v_z(r, z) = -\frac{1}{j\omega\rho_0}\frac{\partial}{\partial z}p(z)\left[1 - \frac{J_0(k_v r)}{J_0(k_v R_h)}\right] + j\omega\xi(x, y)\frac{J_0(k_v r)}{J_0(k_v R_h)}, \tag{4}$$

where J_n denotes the cylindrical Bessel functions of the first kind of order n. After relying on the approximation of the pressure derivative in a very short hole of length h_p

$$\frac{\partial}{\partial z}p(z) \approx \frac{p_{inc} - p_g(x, y)}{h_p}, \tag{5}$$

the mean value of the particle velocity over the cross-section of the hole $S_h = \pi R_h^2$ is

$$\langle v_z(r, z)\rangle_r = \frac{1}{S_h}\iint_{S_h} v_z(r, z)\mathrm{d}S_h \approx -\frac{1}{j\omega\rho_0}\frac{p_{inc} - p_g(x, y)}{h_p}F_{vh} + j\omega\xi(x, y)K_{vh}, \tag{6}$$

with

$$\begin{aligned} F_{vh} &= 1 - K_{vh}, \\ K_{vh} &= \frac{2}{k_v R_h}\frac{J_1(k_v R_h)}{J_0(k_v R_h)}. \end{aligned} \tag{7}$$

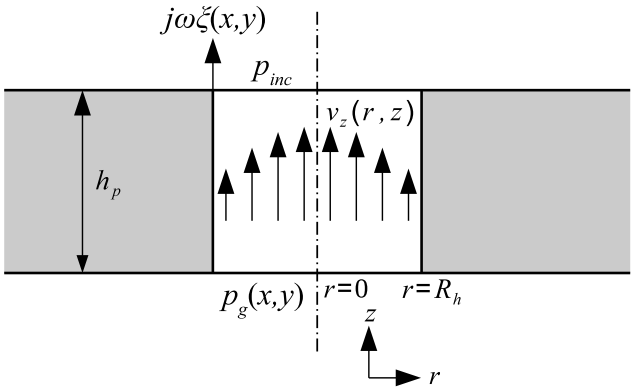

Figure 3. Sketch of the hole in the moving electrode.

The viscous force acting on the interior surface of the hole $2\pi R_h h_p$ is proportional to the normal derivative (here, $\partial/\partial n = -\partial/\partial r$) of the particle velocity (4)

$$F_z = -2\pi R_h h_p \mu\left(\frac{\partial v_z(r, z)}{\partial r}\right)_{r=R_h}, \tag{8}$$

and in using (5) takes the following form

$$F_z(x, y) \approx j\omega\xi(x, y)\Pi_h - \pi R_h^2 K_{vh}\left[p_{inc} - p_g(x, y)\right], \tag{9}$$

with

$$\Pi_h = 2\pi R_h h_p \mu\frac{k_v J_1(k_v R_h)}{J_0(k_v R_h)}. \tag{10}$$

Dividing this force by the area associated with one hole ($4a^2/N$) leads to the equivalent pressure caused by the viscosity effects originating in the hole

$$p_v(x,y) = j\omega\xi(x,y)\Pi_h \frac{N}{4a^2} - \mathcal{R}K_{vh}\left[p_{inc} - p_g(x,y)\right]. \tag{11}$$

2.2.2. Wave Equation Governing the Acoustic Pressure in the Air Gap

In order to express the wave equation for the acoustic pressure $p_g(x,y)$ in the air gap, the following contributions of the mass per unit of time in the gap element of dimensions $\mathrm{d}x \times \mathrm{d}y \times h_g$ have to be taken into account (see velocity contributions in Figure 4):

- Change of the mass per unit of time in both x and y directions $-\frac{\partial}{\partial w}\langle v_{gw}(w,z)\rangle_z \rho_0 \,\mathrm{d}x\,\mathrm{d}y\,h_g$, where w designates x and y.
- Contribution from the moving electrode $-j\omega\xi(x,y)\,\rho_0\,(1-\mathcal{R})\,\mathrm{d}x\,\mathrm{d}y$.
- Contribution form the holes $-\langle v_z(r,z)\rangle_r \rho_0 \mathcal{R}\,\mathrm{d}x\,\mathrm{d}y$, where $\langle v_z(r,z)\rangle_r$ is given by Equation (6).

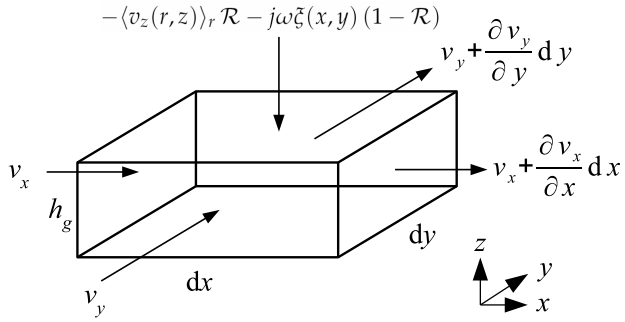

Figure 4. Element of the air gap.

The sum of these terms is equal to $j\omega\,\langle\rho\rangle_z\,\mathrm{d}x\,\mathrm{d}y\,h_g$ (conservation of mass) where $\langle\rho\rangle_z$ is the time-dependent acoustic density in the gap element averaged over the gap thickness. The classical solutions of linearized Navier–Stokes equation and Fourier equation for the heat conduction, under several approximations [29], give, respectively, the particle velocity and temperature variations profiles in the air gap, leading to the relations (after introducing the latter into the gas state equation) $\langle v_{gw}(w,z)\rangle_z = -\frac{1}{j\omega\rho_0}\frac{\partial p_g(x,y)}{\partial w}F_{vg}$ and $\langle\rho\rangle_z = p_g(x,y)\left[\gamma-(\gamma-1)F_{hg}\right]/c_0^2$ [29], with the mean values of the velocity and temperature variation profiles over the air gap thickness given by

$$\begin{aligned} F_{vg} &= 1 - \frac{\tan\left(k_v h_g/2\right)}{k_v h_g/2}, \\ F_{hg} &= 1 - \frac{\tan\left(k_h h_g/2\right)}{k_h h_g/2}, \end{aligned} \tag{12}$$

where k_v is given by (2) and $k_h = \frac{1-j}{\sqrt{2}}\sqrt{\frac{\omega\rho_0 C_p}{\lambda_h}}$. Note that these mean values are calculated for nonslip and isothermal boundary conditions at both (nonperforated) electrodes. Alternatively, the relation accounting for more realistic boundary conditions on the perforated plate [21],

$$F_{(v,h)g} = 1 - \frac{2-\mathcal{R}}{2}\frac{\tan\left(k_{(v,h)}h_g/2\right)}{k_{(v,h)}h_g/2}, \tag{13}$$

can be used.

The combination of the above mentioned terms leads to the wave equation governing the acoustic pressure $p_g(x,y)$ in the air gap

$$\left[\Delta + \chi^2\right] p_g(x,y) = -U(x,y), \tag{14}$$

where the source term is composed from $U(x,y) = U_1\xi(x,y) + U_2 p_{inc}$ with

$$\begin{aligned} U_1 &= \frac{\omega^2\rho_0(1-\mathcal{R}F_{vh})}{F_{vg}h_g}, \\ U_2 &= \frac{F_{vh}\mathcal{R}}{F_{vg}h_g h_p}, \end{aligned} \tag{15}$$

and the complex wavenumber is given by

$$\chi^2 = \frac{\omega^2}{c_0^2}\,\frac{\gamma-(\gamma-1)F_{hg}}{F_{vg}} - \frac{F_{vh}\mathcal{R}}{F_{vg}h_g h_p}. \tag{16}$$

2.2.3. Solution for the Acoustic Pressure in the Air Gap in Case of Piston-like Movement of the Moving Electrode

Since the source term U in (14) does not depend on the spatial coordinates x, y in this case, the solution of (14) takes the classical form

$$p_g(x,y) = A\cos(\kappa_x x)\cos(\kappa_y y) - U/\chi^2, \tag{17}$$

where $\chi^2 = \kappa_x^2 + \kappa_y^2$ (for square geometry $\kappa_x = \kappa_y = \chi/\sqrt{2}$) and A is an integration constant. The boundary condition is given by the acoustic pressure in the peripheral cavity (supposed to be uniform in the whole cavity volume) $p_c = Z_c w_{tot}$, where Z_c is the acoustic impedance of the cavity and w_{tot} is the total volume velocity entering to the cavity. This volume velocity is composed of the volume velocity at the output of the air gap and the volume velocity entering to the cavity through the slits

$$w_{tot} = 8ah_g\left\langle v_{gw}(w,z)\right\rangle_z - S_s\overline{v}_s, \tag{18}$$

where $8ah_g$ is the output surface of the air gap, S_s is the total input surface of the slits, and $\overline{v}_s \cong -\frac{F_{vs}}{j\omega\rho_0}\frac{p_{inc}-p_c}{h_p}$ is the velocity in the slit, with $F_{vs} = 1 - \frac{\tan(k_v h_s/2)}{k_v h_s/2}$ being the mean value of the velocity profile through the thickness of the slit h_s (the influence of the plate velocity on the fluid particle velocity in the slits is supposed to be negligible here). This leads directly to the boundary condition for the normal derivative of the acoustic pressure at the output of the air gap

$$\partial_n p_g = -\Lambda_c p_c + \Lambda_2 p_{inc}, \tag{19}$$

with

$$\Lambda_c = \Lambda_1 + \Lambda_2, \quad \Lambda_1 = \frac{j\omega\rho_0}{8ah_g F_{vg} Z_c}, \quad \Lambda_2 = \frac{S_s F_{vs}}{8ah_g h_p F_{vg}}.$$

The continuity of the acoustic pressure at the boundary between the air gap and the cavity can be approximately expressed using the value at the middle of the square gap side $p_c = p_g(a,0)$ (alternatively, the value at the corner $p_g(a,a)$ or the mean value over the side of the gap could be used). Replacing $\partial_n p_g$ and p_c in (19) by (for example) $\partial_x p_g(a,0)$ and $p_g(a,0)$, respectively, and substituting from the solution (17) readily gives the integration constant

$$A = (A_1\xi + A_2 p_{inc})/A_3, \tag{20}$$

with

$$A_1 = \Lambda_c U_1/\chi^2, \quad A_2 = \Lambda_2 + \Lambda_c U_2/\chi^2, \quad A_3 = \Lambda_c\cos(\kappa_x a) - \kappa_x\sin(\kappa_x a). \tag{21}$$

2.2.4. Solution for the Acoustic Pressure in the Air Gap in Case of Nonuniform Movement of the Moving Electrode

Due to the symmetry of the transducer's geometry, the solution of (14) for nonuniform $U(x,y)$ is expressed here in the first quadrant only (namely, $x,y \in (0,a)$). The chosen Green's function used in the integral formulation for the solution of (14) satisfies the same Neumann's condition (the first derivative vanishes) at $x=0, y=0$ as the solution for the acoustic pressure, which can be expressed as follows [26,27,29]:

$$\begin{aligned} p_g(x,y) = &\int_0^a \int_0^a G(x,x_0;y,y_0)U(x_0,y_0)\mathrm{d}x_0\mathrm{d}y_0 \\ &+ \int_0^a \left[G(x,x_0;y,a)\partial_{y_0}p_g(x_0,a) - \partial_{y_0}G(x,x_0;y,a)p_g(x_0,a)\right]\mathrm{d}x_0 \\ &+ \int_0^a \left[G(x,a;y,y_0)\partial_{x_0}p_g(a,y_0) - \partial_{x_0}G(x,a;y,y_0)p_g(a,y_0)\right]\mathrm{d}y_0, \end{aligned} \tag{22}$$

with the Green's function being given by

$$G(x,x_0;y,y_0) = g(x,x_0;y,y_0) + g(x,-x_0;y,y_0) + g(x,x_0;y,-y_0) + g(x,-x_0;y,-y_0), \tag{23}$$

with

$$g(x,x_0;y,y_0) = -\frac{j}{4}H_0^-\left(\chi\sqrt{(x-x_0)^2+(y-y_0)^2}\right), \tag{24}$$

where H_0^- denotes the cylindrical Hankel function of the second kind of order "0".

Taking into account the boundary condition (19), here without the slits (Λ_2 vanishes), solution (22) becomes

$$p_g(x,y) = \int_0^a \int_0^a G(x,x_0;y,y_0)U(x_0,y_0)\mathrm{d}x_0\mathrm{d}y_0 - p_c I_g(x,y), \tag{25}$$

where

$$\begin{aligned} I_g(x,y) = &\Lambda_1\left[\int_0^a G(x,x_0;y,a)\mathrm{d}x_0 + \int_0^a G(x,a;y,y_0)\mathrm{d}y_0\right] \\ &+ \left[\int_0^a \partial_{y_0}G(x,x_0;y,a)\mathrm{d}x_0 + \int_0^a \partial_{x_0}G(x,a;y,y_0)\mathrm{d}y_0\right]. \end{aligned} \tag{26}$$

The acoustic pressure in the cavity, calculated here as the mean value over the edge of the gap, $p_c = \langle p_g(x,a)\rangle_x$, where $\langle f(w)\rangle_w$ denotes $\int_0^a f(w)\mathrm{d}w/a$, can be then expressed from (25) as follows:

$$p_c = \frac{1}{1+\langle I_g(x,a)\rangle_x}\int_0^a \int_0^a \langle G(x,x_0;a,y_0)\rangle_x U(x_0,y_0)\mathrm{d}x_0\mathrm{d}y_0. \tag{27}$$

2.3. Coupling of the Moving Electrode Displacement Field and the Acoustic Pressure Field

In this section, the strong coupling between the acoustic field inside the transducer, described in previous sections, and the displacement of the moving electrode in the form of an elastically supported rigid perforated plate and a flexible perforated plate clamped at all edges is presented.

2.3.1. Elastically Supported Rigid Perforated Plate

The equation governing the displacement ξ of the elastically supported rigid plate takes the form

$$\left[-M_p\omega^2 + j\omega R_p + K_p\right]\xi = \int_{-a}^a \int_{-a}^a \left[p_g(x,y) - p_{inc} - p_v(x,y)\right]\mathrm{d}x\mathrm{d}y, \tag{28}$$

where M_p is the mass of the plate, K_p is the stiffness of the elastic support, and R_p is the structural damping coefficient which is neglected here (all the damping in the system taken into account here originates in the acoustic fluid-filled parts of the transducer).

Reporting Equations (11) and (17) using (20) to (28) gives, after straightforward calculation, the solution for the displacement of the rigid plate:

$$\xi = \frac{4a^2(1+\mathcal{R}K_{vh})\left[\frac{\sin(\kappa_x a)\sin(\kappa_y a)A_2}{\kappa_x\kappa_y a^2 A_3} - \left(1+\frac{U_2}{\chi^2}\right)\right]p_{inc}}{-M_p\omega^2 + j\omega R_p + K_p + j\omega\pi N + 4a^2(1+\mathcal{R}K_{vh})\left[\frac{U_1}{\chi^2} - \frac{\sin(\kappa_y a)\sin(\kappa_y a)A_1}{\kappa_x\kappa_y a^2 A_3}\right]}. \tag{29}$$

2.3.2. Flexible Perforated Plate Clamped at All Edges

We will depart here from the classical equation governing the displacement of the nonperforated plate [30] with the mass per unit area $M_s = \rho_p h_p$ (ρ_p designates the density of the plate) and the flexural rigidity $D = \frac{Eh_p}{12(1-\nu^2)}$ (E and ν being the Young's modulus and Poisson's ratio, respectively)

$$\left[D\Delta\Delta - M_s\omega^2\right]\xi(x,y) = p_g(x,y) - p_{inc} - p_v(x,y), \tag{30}$$

clamped at all edges

$$\begin{aligned}\xi(x,y) &= \frac{\partial}{\partial x}\xi(x,y) = 0, x = \pm a, \forall y \in (-a,a),\\ \xi(x,y) &= \frac{\partial}{\partial y}\xi(x,y) = 0, y = \pm a, \forall x \in (-a,a).\end{aligned} \tag{31}$$

The displacement field can be searched for in the following form of series expansion (with some truncation in practical implementation):

$$\xi(x,y) = \sum_{mn}\xi_{mn}\psi_{mn}(x,y), \tag{32}$$

where the orthonormal eigenfunctions $\psi_{mn}(x,y)$ satisfy the homogeneous equation associated with Equation (30):

$$\left[\Delta\Delta - k_{m,n}^4\right]\psi_{mn}(x,y) = 0, \tag{33}$$

where $k_{m,n}^4 = (k_{xm}^2 + k_{yn}^2)^2$. An approximate form of such eigenfunctions can be obtained as a series expansion over known functions from numerically (FEM) calculated results using the method described in [31] for nonperforated rectangular clamped plates and in [32] for perforated square clamped plates, the latter being used herein (see Appendix A).

Using the properties of the eigenfunctions [29], the modal coefficients ξ_{mn} in (32) can be obtained from the relation (using Equation (11))

$$\xi_{mn}\left[Dk_{m,n}^4 - M_s\omega^2 + j\omega\Pi_h\frac{N}{4a^2}\right] = (1-\mathcal{R}K_{vh})\int_{-a}^{a}\int_{-a}^{a}\left[p_g(x,y) - p_{inc}\right]\psi_{mn}(x,y)\mathrm{d}x\mathrm{d}y. \tag{34}$$

Using the relation for the acoustic pressure in the air gap $p_g(x,y)$ (25) along with Equations (15) and (32), Equation (34) can be expressed as follows:

$$\left[Dk_{m,n}^4 - M_s\omega^2 + j\omega\Pi_h\frac{N}{4a^2}\right]\xi_{mn} = c_{mn} - \sum_{qr}^{\infty}\xi_{qr}A_{(mn),(qr)}, \tag{35}$$

or in the matrix form

$$[\mathbb{B} - \mathbb{A}]\Xi = \mathbb{C}, \tag{36}$$

where Ξ is the column vector of elements ξ_{mn}, $\mathbb{B}$ is the diagonal matrix of elements $Dk_{m,n}^4 - M_s\omega^2 + j\omega\Pi_h\frac{N}{4a^2}$, $\mathbb{C}$ is the column vector, and $\mathbb{A}$ is the matrix whose elements c_{mn} and $A_{(mn),(qr)}$ are given, respectively, by

$$c_{mn} = p_{inc}\int_{-a}^{a}\int_{-a}^{a}\psi_{mn}(x,y)\left\{U_2\left[\int_0^a\int_0^a G(x,x_0;y,y_0)\mathrm{d}x_0\mathrm{d}y_0 - MI_g(x,y)\right] - 1\right\}\mathrm{d}x\mathrm{d}y, \quad (37)$$

and

$$A_{(mn),(qr)} = U_1\int_{-a}^{a}\int_{-a}^{a}\psi_{mn}(x,y)\left[\int_0^a\int_0^a G(x,x_0;y,y_0)\psi_{qr}(x,y)\mathrm{d}x_0\mathrm{d}y_0 - N_{qr}I_g(x,y)\right]\mathrm{d}x\mathrm{d}y, \quad (38)$$

with

$$\begin{aligned} M &= \frac{1}{1+\langle I_g(x,a)\rangle_x}\int_0^a\int_0^a\langle G(x,x_0;a,y_0)\rangle_x\,\mathrm{d}x_0\mathrm{d}y_0,\\ N_{qr} &= \frac{1}{1+\langle I_g(x,a)\rangle_x}\int_0^a\int_0^a\langle G(x,x_0;a,y_0)\rangle_x\,\psi_{qr}(x_0,y_0)\,\mathrm{d}x_0\mathrm{d}y_0. \end{aligned} \quad (39)$$

Solving Equation (36) for Ξ gives the modal coefficients ξ_{mn} and thus the displacement field of the plate $\xi(x,y)$.

3. Analytical Results and Comparisons with the Numerical (FEM) Ones

In this section, the analytical results calculated using the present method are discussed and compared with the numerical (FEM) results provided by the software Comsol Multiphysics, version 6.0. The numerical formulation for the acoustic field in thermoviscous fluid inside the transducer, involving the acoustic particle velocity $\vec{v}$, acoustic temperature variation τ, and acoustic pressure p using the Acoustics Module [33], was coupled with the classical linear mechanical formulation for the plate provided by the Structural Mechanics Module [34]. One quarter of the transducer geometry was used for the simulation (the rest was symmetric), and the mesh consisted of tetrahedral elements combined with layered prism elements (in the boundary layers). The number of degrees of freedom varied between approximately 1 million and 3 million, depending on the dimensions of the holes in the plate (smaller holes lead to finer mesh and thus higher number of degrees of freedom). The properties of the air used in both numerical and analytical calculations are given in Table 1, and the properties of the material of the plate (silicon) are summarized in Table 2.

Table 1. Properties of the air.

Parameter	Value	Unit
Adiabatic sound speed c_0	343.2	m s^{-1}
Air density ρ_0	1.2	kg m^{-3}
Shear dynamic viscosity μ	1.814×10^{-5}	Pa s
Thermal conductivity λ_h	25.77×10^{-3}	W m^{-1} K^{-1}
Specific heat coefficient at constant pressure per unit of mass C_p	1005	J kg^{-1} K^{-1}
Ratio of specific heats γ	1.4	-

Table 2. Material properties of the plate (silicon).

Parameter	Value	Unit
Plate density ρ_p	2330	kg m^{-3}
Young's modulus E	160	G Pa
Poisson's ratio ν	0.27	-

The displacement of the moving electrode given either by Equation (29) for the elastically supported rigid perforated plate or by Equation (32) for the flexible perforated

plate clamped at all edges was used to calculate the acoustic pressure sensitivity of the electrostatic receiving transducer $\sigma = U_0\overline{\xi}/(h_g p_{inc})$, where $\overline{\xi} = [\iint_{S_e} \xi(x,y)\mathrm{d}S_e]/S_e$ is the mean displacement of the plate over the surface of the backing electrode $S_e = 4a^2$, and U_0 is the polarization voltage (here, $U_0 = 30$ V).

Figure 5 shows the acoustic pressure sensitivity of the receiving transducer with an elastically supported rigid perforated plate of dimensions 0.3×0.3 mm ($a = 150$ µm) and thickness $h_p = 5$ µm with $N = 256$ square holes of side dimension a_h varying between 0.3 µm and 3 µm, as per the thickness of the slits h_s. The air gap thickness is $h_g = 4$ µm, and the peripheral cavity of thickness 50 µm has the volume of $V_c = 2.72 \times 10^{-12}$ m^3. The mass of the plate is given by $M_p = \rho_p h_p(4a^2 - Na_h^2)$, and the structural damping coefficient is supposed to be negligible $R_p = 0$ Ns/m. The stiffness of the elastic support K_p was calculated from the simple numerical model of the mechanical moving part only (*in vacuo*) at very low frequencies. The dimensions of the arms of 145×30 µm lead to $K_p = 200$ N/m. Very good agreement between the analytical results was obtained using the present method (Equation (29)), and the ones provided by the complete numerical model of the transducer can be observed, especially for small a_h and h_s. When the values of a_h and h_s approach the gap thickness h_g (Figure 5d)), the damping seems to be slightly underestimated. Generally, it seems that the "porosity" approach using the ratio $\mathcal{R}$ works better when the dimensions of the holes are much smaller than the gap thickness.

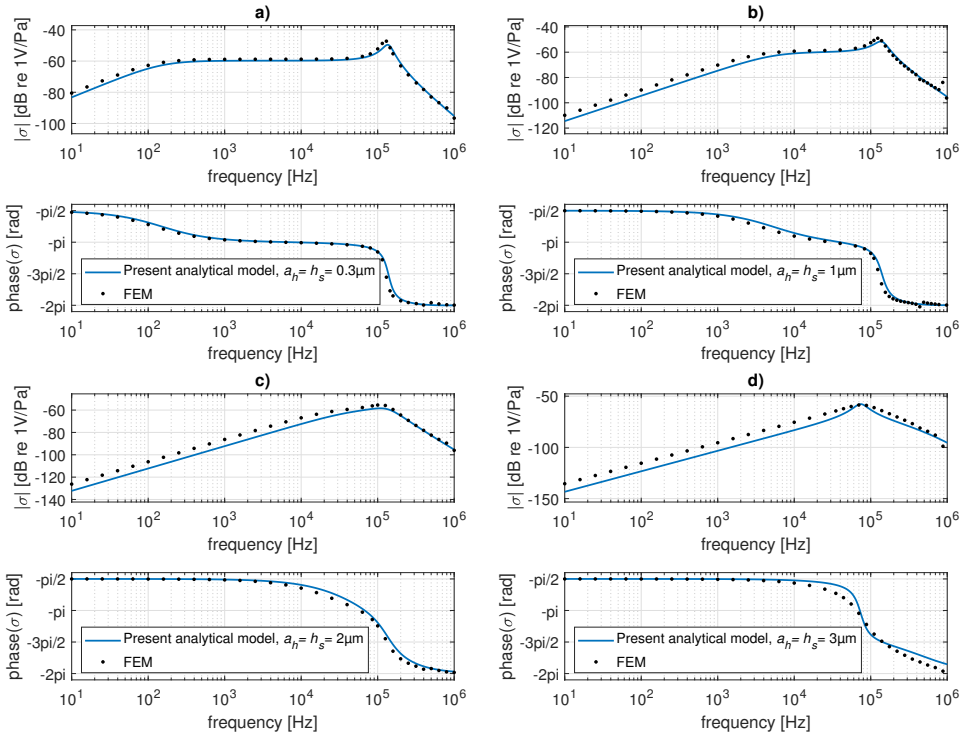

Figure 5. Magnitude (upper curves) and phase (lower curves) of pressure sensitivity of the transducer with elastically supported perforated plate: comparison of the present analytical results (continuous lines) with the numerical (FEM) result (black points) for the side of the holes and the thickness of the slits being equal to (**a**) 0.3 µm, (**b**) 1 µm, (**c**) 2 µm, and (**d**) 3 µm.

The acoustic pressure sensitivities of the receiving transducer with flexible perforated plate clamped at all edges of dimensions $a = 0.5$ mm and thickness $h_p = 10$ µm with $N = 400$ square holes of side dimension a_h varying between 2 µm and 7 µm are shown in Figure 6. Here, the air gap thickness is $h_g = 10$ µm, and the volume of the cavity is $V_c = 10^{-10}$ m^3. The analytical result, calculated using the method described in Section 2.3.2, here takes into account only the first mode of the vibration of the plate ψ_{11} in Equations (37) and (38), which is sufficient in the audio frequency range. Very good

agreement between this analytical result and the reference numerical one can be found in the pass band of the transducer. At very high frequencies, the higher modes of the plate vibrations (not contained in the analytical results) appear in the numerical results.

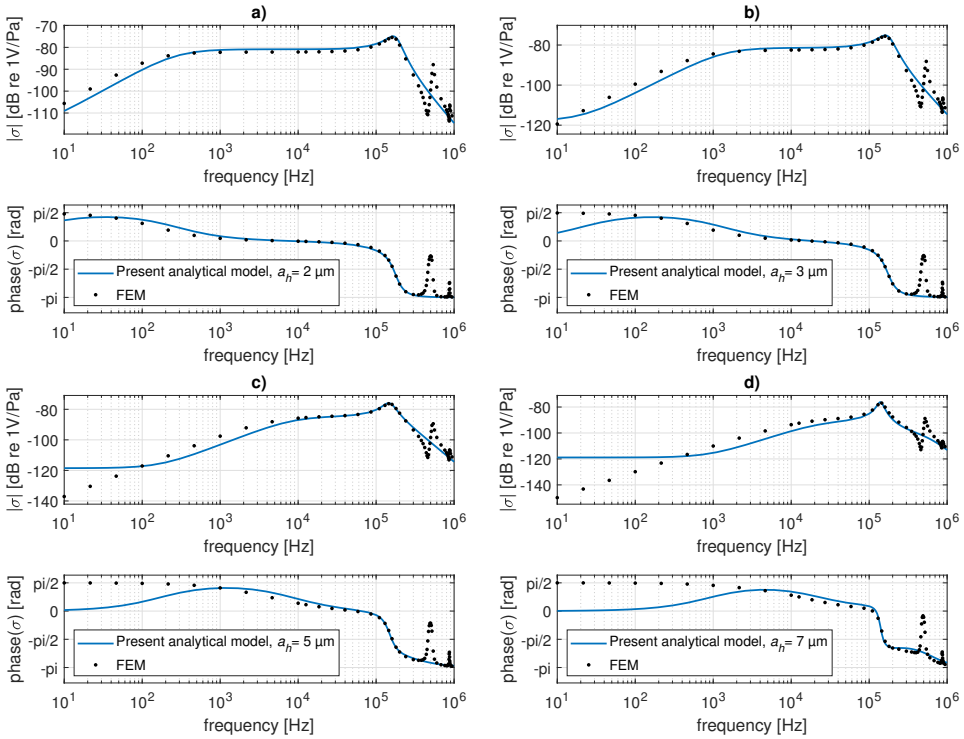

Figure 6. Magnitude (upper curves) and phase (lower curves) of pressure sensitivity of the transducer with flexible perforated clamped plate: comparison of the present analytical results (continuous lines) with the numerical (FEM) result (black points) for the side of the holes being equal to (**a**) 2 μm, (**b**) 3 μm, (**c**) 5 μm, and (**d**) 7 μm.

At very low frequencies, the difference between the acoustic pressure in the gap $p_g(x,y)$ and the incident acoustic pressure p_{inc} is very small due to the acoustic short circuit through the holes (see Figure 7 for $p_{inc} = 1$ Pa and hole side of 2 μm (left) and 5 μm (right) at $f = 100$ Hz). This leads to the numerical noise in the results of the integrals in Equations (25), (37) and (38), especially for larger holes (Figure 7b)). Since this pressure difference is the source for the plate displacement (see Equation (30)), the analytical results are perturbed by the noise in the low-frequency range (see Figure 6c,d). However, when using the transducer in the audio frequency range, the effect of the acoustic short circuit should be reduced, which leads to the use of small holes. For this case, the present analytical model gives correct results (Figure 6a)).

Using the present analytical model, the dimensions of the transducer can be further optimized, as shown in Figure 8. Smaller dimensions of the holes improve the pass band of the transducer in the lower frequency range ($a_h = 1$ μm in Figure 8a). The dependence of the sensitivity σ on the air gap thickness h_g in the pass band of the transducer presents the common sensitivity doubling (+6 dB) when halving the gap thickness for small holes ($a_h = 1$ μm in Figure 8a, $a_h = 2$ μm in Figure 8b), while in the case of larger holes, this effect almost disappears ($a_h = 5$ μm in Figure 8c, $a_h = 7$ μm in Figure 8d). However, the impact of decreasing h_g on increasing damping of the resonance, which is usual in condenser microphones, is preserved in the case of a perforated moving electrode. Note that the thickness of the plate h_p influences the mass and stiffness of the plate, hence the resonance frequency and amplitude of the plate displacement. Higher thickness h_p leads to higher resonance frequency (thus, higher pass band of the transducer) and lower sensitivity.

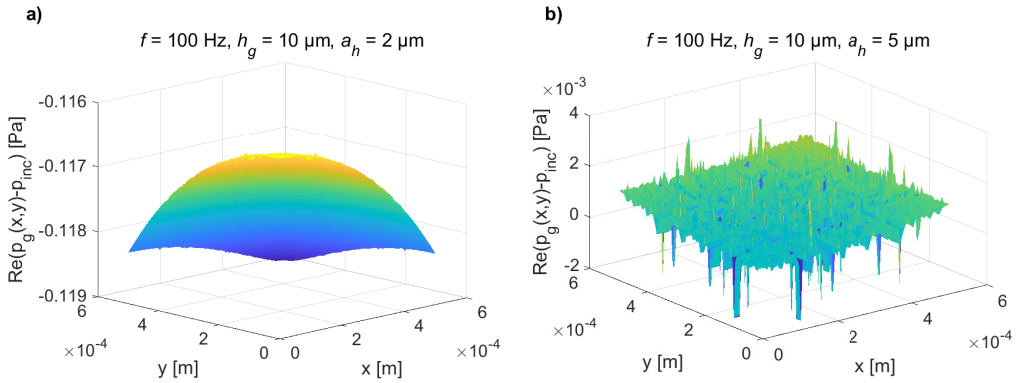

Figure 7. Real part of the difference of the acoustic pressure between both sides of the plate $\Re[p_g(x,y) - p_{inc}]$ in the first quadrant $(x, y \in (0, a))$ calculated using the present method at $f = 100$ Hz for $p_{inc} = 1$Pa and for the side of the holes being equal to (**a**) $a_h = 2$ μm (left) and (**b**) $a_h = 5$ μm (right).

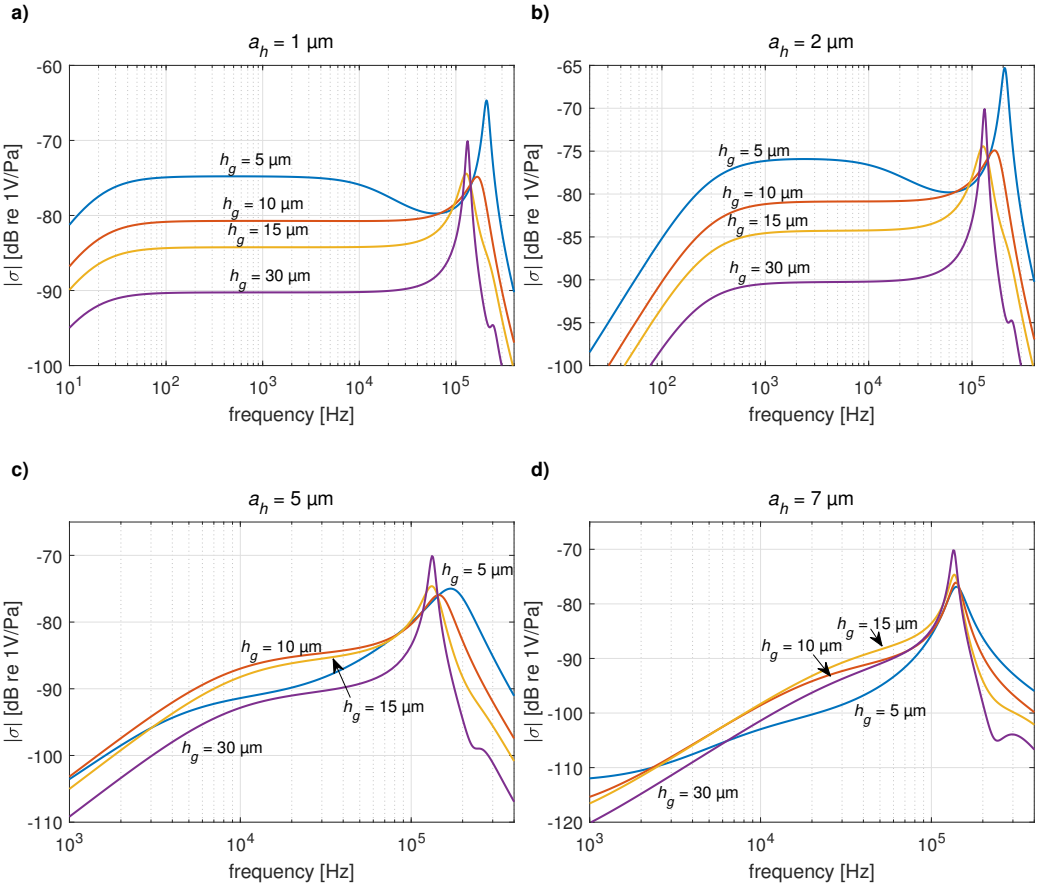

Figure 8. Magnitude of pressure sensitivity of the transducer calculated using the present method: the effect of varying air gap thickness h_g for the side of the holes being equal to (**a**) 1 μm, (**b**) 2 μm, (**c**) 5 μm, and (**d**) 7 μm.

4. Conclusions

The analytical model of an electroacoustic transducer with the moving electrode in the form of a perforated plate (rigid elastically supported or flexible clamped at all boundaries) was developed. The formulation for the acoustic pressure field in the air gap between the moving and the fixed electrode was derived, taking into account the acoustic short circuit

through the holes, the thermal and viscous boundary layers effects in the thin fluid film, and the coupling with the displacement of the plate. The displacement of the plate and the acoustic pressure sensitivity of the transducer used as a microphone was calculated, and the latter was compared to the reference numerical (FEM) results. Very good agreement between these models was found in the transducer pass band, and some discrepancies, appearing generally out of the frequency range of interest, were discussed and explained. The influence of some geometrical parameters of the transducer, such as dimensions of the holes in the plate or air gap thickness, was investigated.

Note that only the first mode of the flexible plate vibration was taken into account here using the analytically expressed approximation of its first eigenfunction calculated numerically. This is sufficient in the audio frequency range; however, further research should focus on improved expression of the eigenfunctions, providing better results at the frequencies above the first resonance, where the higher modes of the perforated plate vibration occur.

Author Contributions: Conceptualization, K.Š. and P.H.; methodology, K.Š. and P.H.; software, K.Š. and P.H.; validation, K.Š. and P.H.; formal analysis, K.Š. and P.H.; investigation, K.Š. and P.H.; resources, K.Š. and P.H.; data curation, K.Š. and P.H.; writing—original draft preparation, K.Š. and P.H.; writing—review and editing, K.Š. and P.H.; visualization, K.Š. and P.H.; supervision, P.H. All authors have read and agreed to the published version of the manuscript.

Funding: This research was funded by the Grant Agency of the Czech Technical University in Prague grant number SGS18/200/OHK2/3T/16. The APC was funded by the Future Fund of the Czech Technical University in Prague (2003).

Data Availability Statement: Not applicable.

Acknowledgments: This work was supported by the Grant Agency of the Czech Technical University in Prague, grant No. SGS18/200/OHK2/3T/16. The authors would like to thank Michel Bruneau from Le Mans University for helpfull discussions.

Conflicts of Interest: The authors declare no conflicts of interest.

Appendix A. Approximate Eigenfunctions of the Perforated Flexible Square Plate Clamped at All Edges [32]

Since no exact analytical expression for the eigenfunctions of perforated plates is known, to our knowledge, the eigenfunctions used in Section 2.3.2 are approximated using the series expansion [32]

$$\psi_{mn}(x,y) = \sum_{qr} c_{(qr),(mn)} \phi_q(x) \phi_r(y), \tag{A1}$$

where the basis functions $\phi_q(x), \phi_r(y)$ are the symmetrical eigenfunctions of 1D beam clamped at both ends, given by [27,35]

$$\phi_q^s(x) = \frac{1}{\sqrt{2}a}\left[\frac{\cos\left(\alpha_q^s x\right)}{\cos\left(\alpha_q^s a\right)} - \frac{\cosh\left(\alpha_q^s x\right)}{\cosh\left(\alpha_q^s a\right)}\right], \quad \text{with} \quad \tan\left(\alpha_q^s a\right) = -\tanh\left(\alpha_q^s a\right), \tag{A2}$$

and similarly for $\phi_r^s(y)$. Such a form of the basis functions ensures that the approximated eigenfunctions $\psi_{mn}(x,y)$ verify the boundary conditions (31). A simple numerical (FEM) simulation of the perforated plate only (not loaded by the acoustic parts of the transducer) was performed in order to obtain the numerically calculated eigenfunctions ${}^n\psi_{mn}(x,y)$. The coefficients $c_{(qr),(mn)}$ in (A1) were then calculated from these numerical eigenfunctions as follows:

$$c_{(qr),(mn)} = \frac{1}{2a^2}\int_{-a}^{a}\int_{-a}^{a} {}^n\psi_{mn}(x,y)\phi_q(x)\phi_r(y)\mathrm{d}x\mathrm{d}y. \tag{A3}$$

Other important information provided by the simple numerical model of the perforated plate are the eigenfrequencies ${}^{n}f_{mn}$ associated with each eigenmode m, n. The eigenvalues k_{xm}, k_{yn} are then expressed from these numerically calculated eigenfrequencies ${}^{n}f_{mn}$ as follows:

$$k_{xm} = \sqrt{\frac{2\pi\ {}^{n}f_{mm}}{2c_p}}, \tag{A4}$$

where $c_p = \sqrt{D/M_s}$ is the wave speed on the plate. Note that k_{yn} has the same values as k_{xm} in the case of a square plate.

References

1. Malcovati, P.; Baschirotti, A. The Evolution of Integrated Interfaces for MEMS Microphones. *Micromachines* **2018**, *9*, 323. [CrossRef] [PubMed]
2. Ali, W.R.; Prasad, M. Piezoelectric MEMS based acoustic sensors: A review. *Sens. Actuator A Phys.* **2020**, *301*, 111756. [CrossRef]
3. Dehé, A. Silicon microphone development and application. *Sens. Actuator A Phys.* **2007**, *133*, 283–287. [CrossRef]
4. Bergqvist, J.; Rudolf, F. A silicon condenser microphone using bond and etch-back technology. *Sens. Actuator A Phys.* **1994**, *45*, 115–124. [CrossRef]
5. Iguchi, Y.; Goto, M.; Iwaki, M.; Ando, A.; Tanioka, K.; Tajima, T.; Takeshi, F.; Matsunaga, S.; Yasuno, Y. Silicon microphone with wide frequency range and high linearity. *Sens. Actuator A Phys.* **2007**, *135*, 420–425. [CrossRef]
6. Scheeper, P.R.; Nordstrand, B.; Gulløv, J.O.; Liu, B.; Clausen, T.; Midjord, L.; Storgaard-Larsen, T. A new measurement microphone based on MEMS technology. *J. Microelectromech. Syst.* **2003**, *12*, 880–891. [CrossRef]
7. Füldner, M.; Dehé, A. Dual Back Plate Silicon MEMS microphone: Balancing High Performance! In Proceedings of the DAGA 2015, Nürnberg, Germany, 16–19 March 2015; pp. 41–43.
8. Peña-García, N.N.; Aguilera-Cortés, L.A.; Gonzáles-Palacios, M.A.; Raskin, J.-P.; Herrera-May, A.L. Design and Modeling of a MEMS Dual-Backplate Capacitive Microphone with Spring-Supported Diaphragm for Mobile Device Applications. *Sensors* **2018**, *18*, 3545. [CrossRef]
9. Rong, Z.; Zhang, M.; Ning, Y.; Pang, W. An ultrasound-induced wireless power supply based on AlN piezoelectric micromachined ultrasonic transducers. *Sci. Rep.* **2022**, *12*, 16174. [CrossRef]
10. Pinto, R.M.R.; Gund, V.; Dias, R.A.; Nagaraja, K.K.; Vinayakumar, K.B. CMOS-Integrated Aluminum Nitride MEMS: A Review. *J. Microelectromech. Syst.* **2022**, *31*, 500–523. [CrossRef]
11. Lynes, D.D.; Chandrahalim, H. Influence of a Tailored Oxide Interface on the Quality Factor of Microelectromechanical Resonators. *Adv. Mater. Interfaces* **2023**, *10*, 2202446. [CrossRef]
12. Verdot, T.; Redon, E.; Ege, K.; Czarny, J.; Guianvarc'h, C.; Guyader, J.-L. Microphone with planar nano-gauge detection: Fluid-structure coupling including thermo-viscous effects. *Acta Acust. United Acust.* **2016**, *102*, 517–529. [CrossRef]
13. Rufer, L.; De Pasquale, G.; Esteves, J.; Randazzo, F.; Basrour, S.; Somà, A. Micro-acoustic source for hearing applications fabricated with 0.35 µm CMOS-MEMS process. *Procedia Eng.* **2015**, *120*, 944–947. [CrossRef]
14. Ganji, B.A.; Sedaghat, S.B.; Roncaglia, A.; Belsito, L. Design and fabrication of very small MEMS microphone with silicon diaphragm supported by Z-shape arms using SOI wafer. *Solid State Electron.* **2018**, *148*, 27–34. [CrossRef]
15. Ganji, B.A.; Majlis, B.Y. Design and fabrication of a new MEMS capacitive microphone using a perforated aluminum diaphragm. *Sens. Actuator A Phys.* **2009**, *149*, 29–37. [CrossRef]
16. Ganji, B.A.; Sedaghat, S.B.; Roncaglia, A.; Belsito, L. Design and fabrication of high performance condenser microphone using C-slotted diaphragm. *Microsyst. Technol.* **2018**, *24*, 3133–3140. [CrossRef]
17. Sedaghat, S.B.; Ganji, B.A.; Ansari, R. Design and modeling of a frog-shape MEMS capacitive microphone using SOI technology. *Microsyst. Technol.* **2018**, *24*, 1061–1070. [CrossRef]
18. Škvor, Z. On the Acoustical Resistance due to Viscous Losses in the Air Gap of Electrostatic Transducers. *Acustica* **1967**, *19*, 295–299.
19. Estèves, J.; Rufer, L.; Ekeom, D.; Basrour, S. Lumped-parameters equivalent circuit for condenser microphones modeling. *J. Acoust. Soc. Am.* **2017**, *142*, 2121–2132. [CrossRef]
20. Zuckerwar, A.J. Theoretical response of condenser microphones. *J. Acoust. Soc. Am.* **1978**, *64*, 1278–1285. [CrossRef]
21. Lavergne, T.; Durand, S.; Bruneau, M.; Joly, N. Dynamic Behavior of Circular Membrane and An Electrostatic Microphone: Effect of Holes In The Backing Electrode. *J. Acoust. Soc. Am.* **2010**, *128*, 3459–3477. [CrossRef]
22. Lavergne, T.; Durand, S.; Bruneau, M.; Joly, N. Analytical Modeling of Electrostatic Transducers in Gases: Behavior of Their Membrane and Sensitivity. *Acta Acust. United Acust.* **2014**, *100*, 440–447. [CrossRef]
23. Naderyan, V.; Raspet, R.; Hickey, C. Thermo-viscous acoustic modeling of perforated micro-electro-mechanical systems (MEMS). *J. Acoust. Soc. Am.* **2020**, *148*, 2376–2385. [CrossRef] [PubMed]
24. Pedersen, M.; Olthuis, W.; Bergveld, P. On the electromechanical behaviour of thin perforated backplates in silicon condenser microphones. In Proceedings of the 8th International Conference on Solid-state Sensors ancl Actuators, and Eurosensors IX, Stockholm, Sweden, 25–29 June 1995; p. 234 A7.

25. Novak, A.; Honzík, P.; Bruneau, M. Dynamic behaviour of a planar micro-beam loaded by a fluid-gap: Analytical and numerical approach in a high frequency range, benchmark solutions. *J. Sound Vib.* **2017**, *401*, 36–53. [CrossRef]
26. Honzík, P.; Bruneau, M. Acoustic fields in thin fluid layers between vibrating walls and rigid boundaries: Integral method. *Acta Acust. United Acust.* **2015**, *101*, 859–862. [CrossRef]
27. Šimonová, K.; Honzík, P.; Bruneau, M.; Gatignol, P. Modelling approach for MEMS transducers with rectangular clamped plate loaded by a thin fluid layer. *J. Sound Vib.* **2020**, *473*, 115246. [CrossRef]
28. Herring Jensen, M.J.; Sandermann Olsen, E. Virtual prototyping of condenser microphone using the finite element method for detailed electric, mechanic, and acoustic characterisation. *Proc. Meet. Acoust.* **2013**, *19*, 030039.
29. Bruneau, M.; Scelo, T. *Fundamentals of Acoustics*; ISTE: London, UK, 2006.
30. Leissa, A.W. *Vibration of Plates*; Scientific and Technical Information Division, National Aeronautics and Space Administration: Washington, DC, USA, 1969.
31. Šimonová, K.; Honzík, P.; Joly, N.; Durand, S.; Bruneau, M. Modelling of a MEMS transducer using approximate eigenfunctions of a square clamped plate. In Proceedings of the 23rd International Congress on Acoustics, Aachen, Germany, 9–13 September 2019; pp. 7361–7368.
32. Šimonová, K.; Honzík, P.; Joly, N.; Durand, S.; Bruneau, M. Modelling of a MEMS Transducer with a Moving Electrode in Form of Perforated Square Plate. In Proceedings of Forum Acusticum 2020, Lyon, France, 7–11 December 2020; pp. 2539–2542.
33. COMSOL Multiphysics. Acoustics Module User's Guide. 2022. Available online: https://doc.comsol.com/6.1/doc/com.comsol.help.aco/AcousticsModuleUsersGuide.pdf (accessed on 23 March 2023).
34. COMSOL Multiphysics. Structural Mechanics Module User's Guide. 2022. Available online: https://doc.comsol.com/6.1/doc/com.comsol.help.sme/StructuralMechanicsModuleUsersGuide.pdf (accessed on 23 March 2023).
35. Le Van Suu, T.; Durand, S.; Bruneau, M. On the modelling of a clamped plate loaded by a squeeze fluid film: Application to miniaturized sensors. *Acta Acust. United Acust.* **2010**, *96*, 923–935. [CrossRef]

Disclaimer/Publisher's Note: The statements, opinions and data contained in all publications are solely those of the individual author(s) and contributor(s) and not of MDPI and/or the editor(s). MDPI and/or the editor(s) disclaim responsibility for any injury to people or property resulting from any ideas, methods, instructions or products referred to in the content.